American Mineralogist, Volume 83, pages 1100–1110, 1998

Scheelite-powellite and paraniite-(Y) from the Fe-Mn deposit at Fianel, Eastern Swiss Alps

JOËL BRUGGER,[1,*] RETO GIERÉ,[2] BERNARD GROBÉTY,[3] AND EVGENY USPENSKY[4]

[1]Institut für Mineralogie und Petrographie, Universität Basel, Bernoullistr. 30, 4056 Basel, Switzerland
[2]Department of Earth and Atmospheric Sciences, Purdue University, West Lafayette, Indiana 47907-1397, U.S.A.
[3]Institute for Geology, Aarhus University, Ole Worms Alle, Bygning 12, 8000 Aarhus, Denmark
[4]IGEM of Russian Academy of Sciences, Staromonetny Per. 35, Moscow 109017, Russia

ABSTRACT

Small syngenetic exhalative Fe-Mn deposits embedded in Triassic marbles of the Suretta, Starlera, and Schams nappes (Eastern Swiss Alps) were subjected to a Tertiary regional metamorphism under blueschist- to greenschist-facies conditions. In one of the deposits (at Fianel, Val Ferrera), this polyphase metamorphism led to the formation of quartz+dolomite veinlets containing beryl, scheelite-powellite, paraniite-(Y), monazite-(Ce), fluorapatite, bergslagite, fluor-roméite, and antimonian betafite; these veinlets crosscut dolomite breccia lenses that are embedded in hematite-quartz-carbonate ores. Scheelite-powellite displays a continuous range of compositions between 28 and 70 mol% $CaMoO_4$; its As_2O_5 contents range from 0.73 to 3.96 wt%, and are positively correlated with the Y_2O_3 contents that vary between 0.33 and 2.47 wt%. The scheelite-powellite grains display a two-stage chemical zoning: stage A generally produced a core and a rim that, relative to the core, is richer in W, As, and Y. During the second stage (stage B), W-rich scheelite-powellite replaces stage-A grains along fractures and rims. Crystals of paraniite-(Y), ideally $(CaWO_4)_2 \cdot YAsO_4$, occur as small inclusions ($=1$ μm) in stage-B scheelite-powellite. The Fianel deposit is only the second locality where paraniite-(Y) has been reported. The paraniite-(Y) from Fianel displays, like the type material, no polysomatic stacking fault in the scheelite-$YAsO_4$ layering. At Fianel, paraniite-(Y) is characterized by elevated Mo contents, and seems to have crystallized under influence of W- and LREE-rich fluids during stage B, i.e., during the metasomatic replacement of Y- and As-rich scheelite-powellite produced in stage A.

INTRODUCTION

A metamorphosed Fe-Mn deposit from the Eastern Swiss Alps contains scheelite-powellite in association with paraniite-(Y). The former was identified by Graeser (1974) in a sample from the dumps of the Fianel mine, Val Ferrera (Graubünden, Switzerland), whereas paraniite-(Y) was discovered during a systematic study of the Fe-Mn deposits in Val Ferrera (Brugger 1996).

Scheelite, $CaWO_4$, is the most important economic tungsten mineral. It appears in a wide variety of environments, including metamorphic stratabound deposits, hydrothermal veins, and skarns. Scheelite forms a complete solid solution with powellite, $CaMoO_4$ (Tyson et al. 1988), but natural specimens rarely contain >4 mol% $CaMoO_4$. According to Hsu and Galli (1973), this observation indicates that Mo is removed as molybdenite (MoS_2) in most geological environments favorable to scheelite formation. Therefore, crystallization of ''scheelite-powellite'' requires low S_2 fugacities and/or oxidizing conditions.

Electron microprobe (EMP) analyses of scheelite-powellite from Fianel revealed unusually high contents of As and rare earth elements (REE; this abbreviation here includes the lanthanides and Y). REE substitute for Ca^{2+} in the scheelite structure (Cottrant 1981). Although most scheelites contain <2000 ppm REE, up to 2.0 wt% REE_2O_3 are present in some cases (Semenov 1963) and Hsu and Galli (1973) reported up to 0.3 wt% Y in scheelite-powellite (with <4 mol% $CaMoO_4$) from hydrothermal veins. During precipitation, scheelite concentrates REE, whereby the enrichment relative to the fluid is about 4–5 times greater for Lu than for La (Raimbault et al. 1993). In certain situations, however, elevated REE contents in scheelites are due to the presence of microscopic inclusions of different REE-bearing minerals [e.g., monazite-(Ce), xenotime-(Y), apatite, fluorite; cf. Ivanova et al. 1987]. In contrast to the REE, there is very little information about As in scheelite, although scheelite commonly occurs together with arsenic minerals (e.g., arsenopyrite). Richard et al. (1981), for example, were unable

* Present address: VIEPS, Department of Earth Sciences, Monash University, Clayton, Victoria 3168, Australia. E-mail: joelb@artemis.earth.monash.edu.au

0003–004X/98/0910–1100$05.00

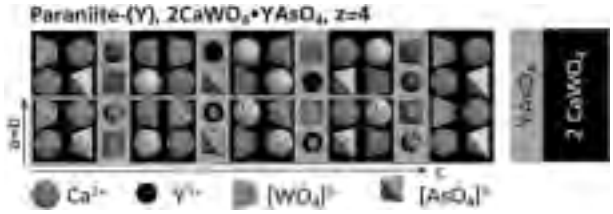

FIGURE 1. Structure of paraniite-(Y) after Demartin et al. (1992). The structure consists of a regular stacking of two scheelite layers (black) and one $YAsO_4$ layer (gray). The vertical displacements along the $a = b$ axis are indicated (½ or 0).

to detect As in scheelites from various Alpine deposits (i.e., <10 ppm).

Paraniite-(Y) was discovered in a sample from an Alpine vug in the Pizzo Cervandone area, Penninic Alps, Italy (Demartin et al. 1994). The formula of paraniite-(Y) from the type locality was given as $(Ca_{1.64}REE_{0.36})(REE)[(As_{0.96},W_{0.04})O_4][(W_{0.89},As_{0.11})O_4]_2$, or simplified as $(CaWO_4)_2 \cdot YAsO_4$. The mineral has a layered structure consisting of a regular stacking of two scheelite layers and one $YAsO_4$ layer (Fig. 1). The $YAsO_4$ layer has a scheelite structure, and thus is different from chernovite-(Y), also $YAsO_4$, which exhibits a zircon structure (Table 1). Chernovite-(Y) undergoes a transition to the scheelite structure at high pressure (Demartin et al. 1994). In paraniite-(Y), the occurrence of $YAsO_4$ layers with the scheelite structure is not related to a pressure effect, but is an example of stabilization of this polymorph by the structural effect (Demartin et al. 1994).

The aim of this paper is to document the anomalous As and REE contents of scheelite-powellite. Furthermore, we will discuss textural and crystal-chemical relationships between scheelite-powellite and paraniite-(Y). This mineral association has been studied using various analytical methods, at scales ranging from the outcrop to unit cell. Particular attention has been given to the relations between the different scales of observation and how each one of these contributes to the understanding of this unique mineral association.

REGIONAL GEOLOGICAL FRAMEWORK

The Suretta, Starlera, and Schams nappes belong to the Middle Penninic domain (Briançonnais) of the Eastern Swiss Alps, generally characterized by shallow water sedimentation during the Mesozoic (Trümpy 1980). The Triassic marbles of the Suretta, Starlera, and Schams nappes host many small stratiform Fe-Mn deposits (Stucky 1960). Ores containing hematite, quartz, and carbonate, as well as some muscovite, fluorapatite, and strontian barite are most common. In some of the deposits, complex Mn and Fe-Mn ores occur, and minerals such as braunite, jacobsite, rhodonite, tephroite, rhodochrosite, aegirine, spessartine, calderite, medaite, barylite, and strontian barite have been identified. Ore pebbles in synsedimentary Mesozoic breccias indicate that the ores were formed early during sedimentation or diagenesis of the Triassic carbonates. Based on geochemical and textural evidence, Brugger (1996) inferred a syngenetic exhalative origin for these deposits. Both deposits and host rocks have undergone a polyphase Tertiary regional metamorphism characterized by four deformation events (Schmid et al. 1997). The main deformation, D_1 (Ferrera phase) took place at blueschist- to greenschist-facies conditions, and is associated with isoclinal folding and a pervasive schistosity S_1. The second phase, D_2 (Niemet phase) occurred under greenschist-facies conditions; it is also associated with isoclinal folding, but an axial plane schistosity S_2 developed only in the most incompetent rock types. The subsequent phase (D_3) produced a crenulation in the most incompetent rocks and finally, a brittle event (D_4) caused subvertical N-S-striking faults.

THE FE-MN DEPOSIT AT FIANEL

The Triassic marbles at Fianel belong to the Starlera nappe and host a lenticular ore body ($60 \times 60 \times 20$ m), which had been exploited for Fe until the end of the 19th century. It is the largest and best-exposed deposit of the region. The scheelite-powellite occurrence is restricted to a relatively small outcrop (Fig. 2a), where the richest mineralization is hosted by a stratiform breccia lens, which is embedded in hematite-quartz-carbonate ores (Figs. 2a and 3). Two additional mineralized breccia lenses occur above the larger main lens (Fig. 2a). The breccia consists of angular fragments of pink manganoan dolomite (2–4.5 mol% $MnCO_3$ and 0.2–0.6 mol% $FeCO_3$), which are cemented by quartz, hematite, carbonate, and minor strontian barite and talc. It is crosscut by numerous veinlets of quartz+dolomite (Fig. 3). The chemical composition of dolomite from these veins is similar to that of the pink dolomite clasts in the breccia. The most typical accessory mineral of the quartz+dolomite veinlets is blue beryl (up to 3 cm in length; cf. Stucky 1960) with a composition that is characteristic of beryls from ''Alpine vugs'' (i.e., high contents of Na, Mg, and Fe, but low in Sc, Mn, and Ti; cf. Hänni 1980). Most beryl crystals are

TABLE 1. Physical properties of the minerals of interest

	Scheelite	Powellite	Paraniite-(Y)	Chernovite-(Y)
Formula	$CaWO_4$	$CaMoO_4$	$2CaWO_4 \cdot YAsO_4$	$YAsO_4$
Space Group	$I4_1/a$	$I4_1/a$	$I4_1/a$	$I4_1$
a [Å]	5.243	5.224	5.135	7.039
c [Å]	11.376	11.430	33.882	6.272
Density [g/cm³]	6.12	4.25	5.95	4.87
Reference	Zalkin and Templeton (1964)	Dana and Dana (1951)	Demartin et al. (1992)	Goldin et al. (1968)

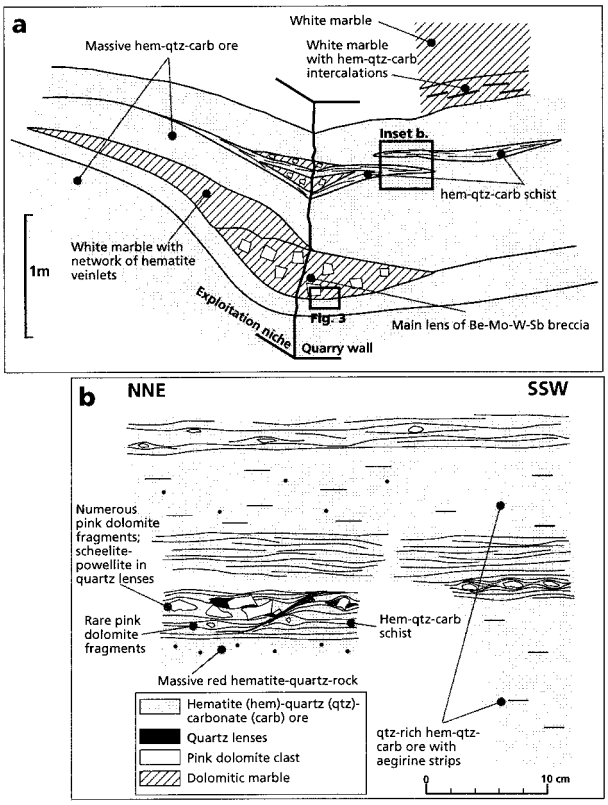

FIGURE 2. Geometry of the scheelite-powellite-bearing mineralization at Fianel, Val Ferrera (Central Alps, Switzerland).

broken, whereby the fractures are filled by quartz+carbonate. In addition to beryl, the quartz+dolomite veinlets contain yellow scheelite-powellite, strontian barite, isolated brownish fluor-roméite grains (locally with antimonian betafite cores; Brugger et al. 1997), fluorapatite, and rare bergslagite. Fluorapatite contains up to 0.09 wt% Ce_2O_3, but its MnO, Na_2O, and FeO contents are below 0.05 wt%. The rim of some fluorapatite crystals shows replacement textures, in which As_2O_5 (up to 3.36 wt%) and SrO (up to 0.29 wt%) are enriched relative to the core. Scheelite-powellite locally hosts small (<10 μm) thorian monazite-(Ce) inclusions. Some vugs in the veinlets contain idiomorphic crystals of quartz, dolomite, and barite, green crusts of nearly pure powellite, and rare aggregates of white acicular chernovite-(Y).

In the vicinity of the breccia lenses, the schistose hematite-quartz-carbonate ores contain small pink dolomite clasts (=1.5 cm; Fig. 2b), in which anhedral phenakite crystals occur (Be_2SiO_4, identified on the basis of X-ray powder diffraction patterns obtained with a Gandolfi camera). The phenakite crystals are up to 600 μm across and were formed during or after D_1. Some of the isolated pink dolomite clasts were isoclinally folded during D_1, indicating a pre-D_1 age for the brecciation. Shear bands penetrate into the breccia (Fig. 3) and support this interpretation. Quartz masses, which contain scheelite-powellite in some cases, formed in the pressure shadows of the

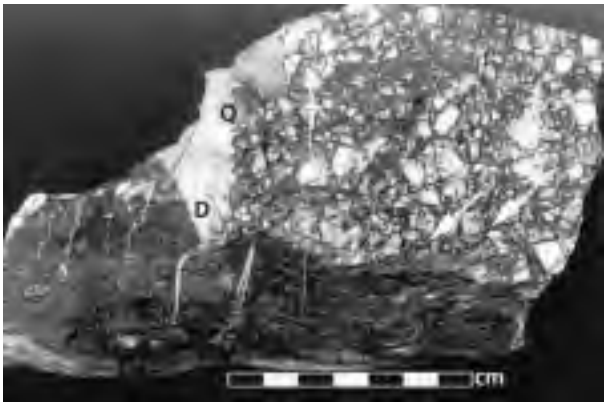

FIGURE 3. Contact between the main pink dolomite breccia and the dark embedding hematite-quartz-carbonate ore. The discordant quartz (Q) + dolomite (D) veinlets contain the Be-, Mo-, W-, and Sb-minerals. Shear bands penetrating the breccia are indicated by arrows.

clasts. The relative age of these masses is unknown; at Fianel, D_1 and D_2 are almost coaxial, and it is difficult to attribute the pressure shadow fillings to one or the other event. The Be-, Mo-, W-, and Sb-bearing quartz+dolomite veins in the breccia lenses are clearly discordant with respect to S_1, and their contacts are sharp and not deformed. Quartz, dolomite, and scheelite-powellite commonly are elongated parallel to the opening direction of the veinlets. The three minerals therefore crystallized simultaneously with the opening of the fracture. Because the veinlets do not show the N-S orientation typical of D_4, and because they clearly crosscut D_1 structures, they must have been formed sometime after D_1 but before D_4.

SCHEELITE-POWELLITE AT THE SCALE OF THE ELECTRON MICROPROBE

Analytical methods

Scheelite-powellite grains were isolated under a binocular microscope, embedded in epoxy resin, and then polished. The chemical zonation was studied using backscattered electron (BSE) images, which depict differences in the mean atomic number at the surface of the sample. In scheelite-powellite, this method mainly maps the substitution of Mo by the heavier W; consequently, Mo-rich zones appear darker than W-rich zones. The BSE pictures were obtained at the central SEM Laboratory of the University of Basel.

EMP analyses were performed with a CAMECA SX-50 instrument at the Institute for Mineralogy and Petrography of the University of Bern. The analytical conditions used are listed in Table 2, and the positions of background measurements were chosen on the basis of qualitative wavelength dispersive spectra. W has numerous peaks that interfere with some of the REE lines. In particular, strong interferences precluded the determination of Ce_2O_3 at levels <1 wt% [Ce-$L\alpha \approx 2^{nd}$ order W-$L\beta_1$ (on LiF), Ce-$L\beta_1 \approx 2^{nd}$ order As-$K\beta_1$ (on LiF), Ce-$M\alpha_1 \approx 2^{nd}$ order

TABLE 2. Analytical conditions for the EMP analysis of scheelite-powellite from Fianel

Element	Line	Standard	Xtal	Cond.	Pk. time	+BG	−BG
Ca	$K\alpha$	Scheelite (nat)	PET	no. 1	15	400	500
W	$L\alpha$	Scheelite (nat)	LiF	no. 1	15	500	500
Mo	$L\alpha$	Powellite (syn)	PET	no. 1	15	500	680
As	$L\alpha$	Adamite (nat)	TAP	no. 1	30	500	500
Y	$L\alpha$	Y_2O_3 (syn)	TAP	no. 1	30	400	400
Nd	$L\alpha$	Glass (syn)	LiF	no. 2	120	180	850
La	$L\alpha$	Glass (syn)	LiF	no. 2	120	500	250
Sm	$L\beta$	Glass (syn)	LiF	no. 2	120	350	450
Dy	$L\beta$	Glass (syn)	LiF	no. 2	120	200	200
Er	$L\alpha$	Glass (syn)	LiF	no. 2	120	230	300

Notes: Standards: nat = natural, syn = synthetic; Xtal = Detector crystal; Cond.: analytical condition no. 1 = 15 kV, 20 nA; condition no. 2 = 25 kV, 200 nA. Pk. time = time (in seconds) counted on peak. BG = the shift, relative to the position of the analyzed line, for background measurement, given in sin θ*10 000 units.

W-$M\alpha_1$ (on TAP)]. The measured REE show no interference with W and no significant overlap with other REE. Element distribution maps were generated with a JEOL 8600 Superprobe (wavelength dispersive mode, 15 kV and 45 nA) at the Geophysical Laboratory, Carnegie Institution of Washington.

Morphology

The complex zonation patterns (Fig. 4) observed in scheelite-powellite from Fianel may be separated into two morphological types, which correspond to two successive events in the crystallization history of this mineral. The main episode of growth (stage A) produced one or two zones of scheelite-powellite; in the latter case, we can distinguish a Mo-rich core (A_1), separated by a sharp boundary from the rim (A_2; Figs. 4a and 5a). Both zones appear homogeneous on BSE images. At a later stage (stage B), scheelite-powellite developed within or around stage-A scheelite-powellite: stage-B zones display veinlike textures that point to a metasomatic replacement of stage-A scheelite-powellite along fractures or grain boundaries (Figs. 5a and 5b).

In the grain depicted in Figures 4a and 5b, a relatively thick stage-B veinlet displays an outer, W-rich zone B_1, and a narrow Mo-richer inner zone B_2, thus documenting an evolution toward Mo-richer compositions during formation of this stage-B vein. The crystal shown in Figure 4b contains three generations of stage-B veinlets: A dense network of thin veinlets (B_0) is crosscut by a vein (arrow in Fig. 4b), which evolves from W-rich toward Mo-rich compositions (B_1 and B_2, respectively). Thin B_1 and B_2 veinlets propagate from this vein (cf. schematic inset in Fig. 4b). The same succession is also visible in an enlarged BSE view of the crystal (Fig. 4c), where B_2 appears as a patch around a quartz inclusion (black). In the circle on Figure 4b, a B_2 scheelite-powellite patch similarly propagates from a quartz inclusion and crosscuts B_1 veinlets.

In summary, scheelite-powellite of stage A mostly displays two concentric zones, the older one (A_1) being

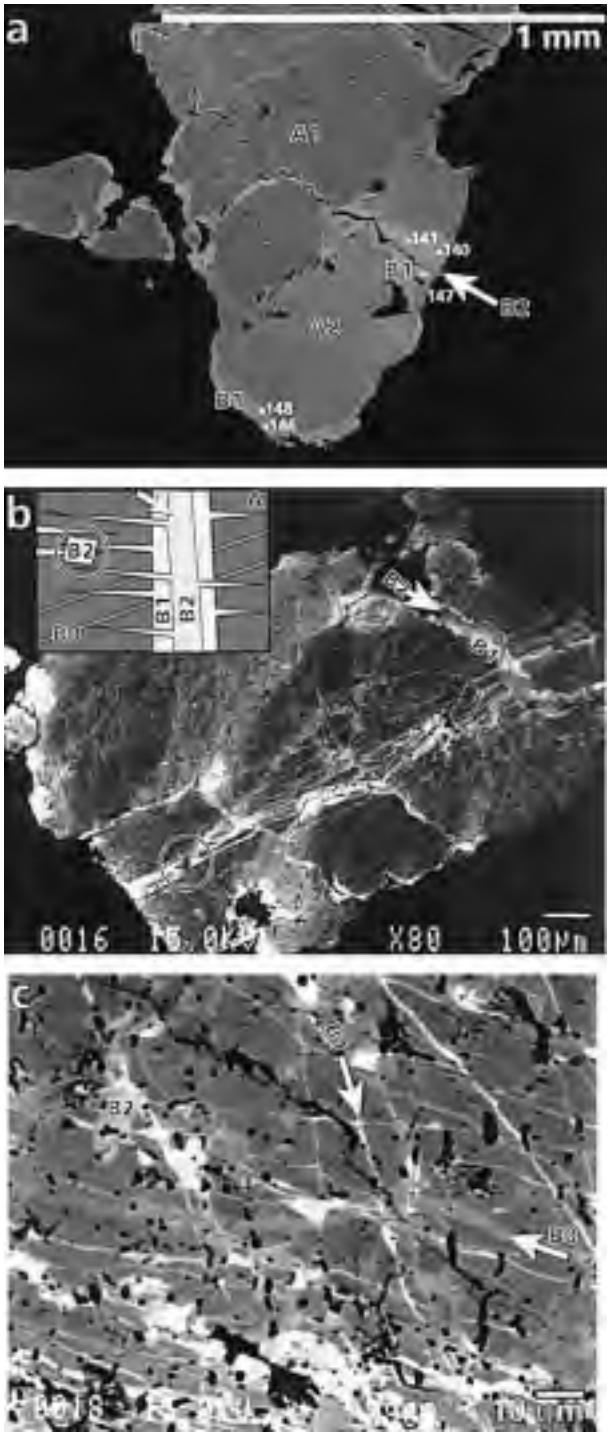

FIGURE 4. BSE pictures of scheelite-powellite grains from Fianel, Val Ferrera. (**a**) Crystal Se2/10, whose morphology is illustrated schematically in Figure 5. The numbers indicate analyses listed in Table 3; (**b**) Mo-rich scheelite-powellite crystal crosscut by several generations of W-rich veinlets; the inset schematically shows the relations between the different generations of veinlets; circle and arrow are explained in text; (**c**) high magnification view of the crystal shown in Figure 4b.

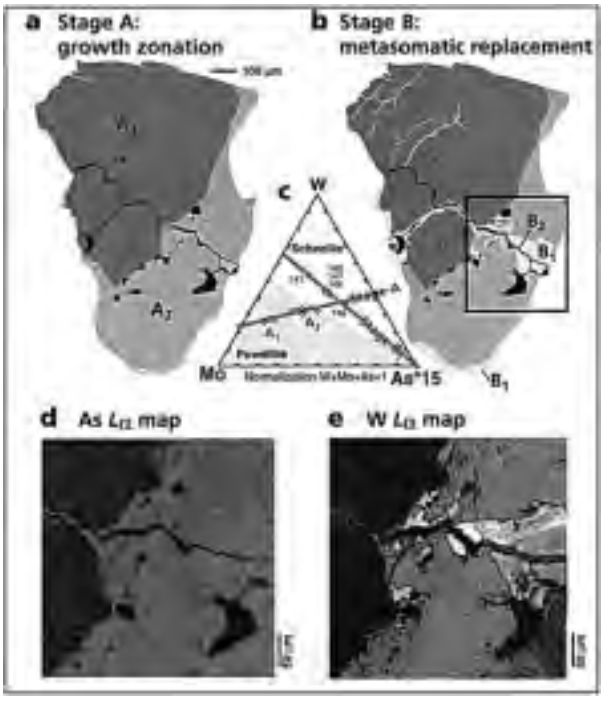

FIGURE 5. Zonation of scheelite-powellite grain Se2/10, which formed during two stages: (**a**) view of the crystal at the end of stage A; (**b**) view of the crystal at the end of stage B; (**c**) EMP analyses plotted in a W-Mo-As*15 diagram; the numbers refer to the analyses listed in Table 3 and shown in Figure 4a; (**d**) arsenic distribution in the area indicated by a rectangle on Figure 5b; (**e**) tungsten distribution of the same area.

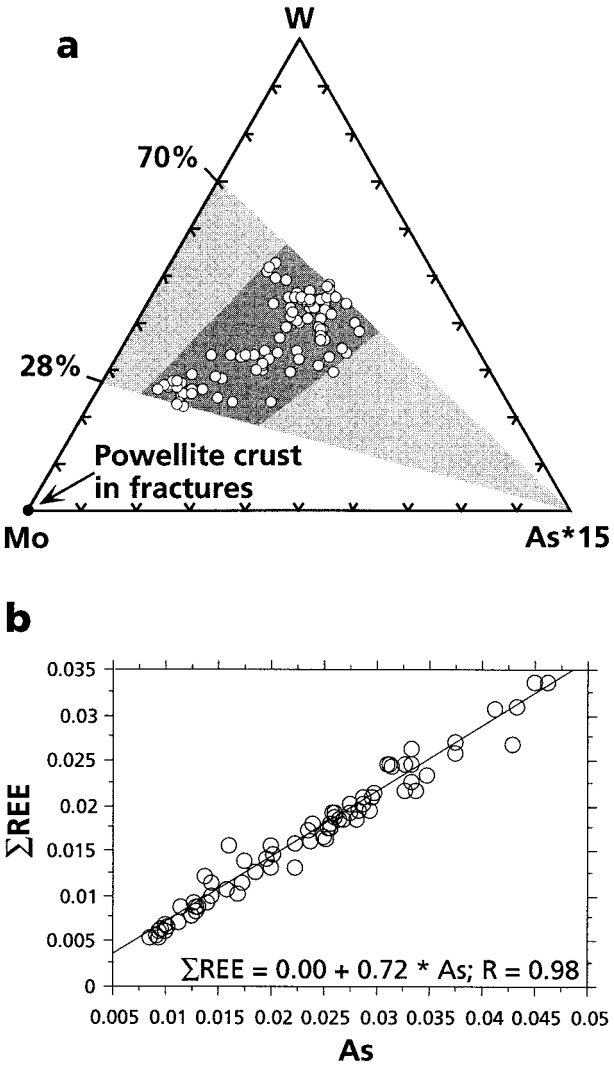

FIGURE 6. (**a**) Triangular plot of all EMP analyses of scheelite-powellite from Fianel (molar proportions). (**b**) a plot of formula proportions of ΣREE vs. As (normalized to four O atoms).

richer in Mo. At least three generations of stage-B scheelite-powellite can be distinguished: the first one (B_0) is richest in Mo, the second (B_1) is richest in W, and the last one (B_2) is of intermediate composition. Veinlets showing transition in composition between B_1 and B_2 also occur locally.

Chemical composition

Scheelite-powellite from Fianel exhibits a continuous range of compositions between 28 and 70 mol% $CaWO_4$ (Fig. 6a). It is characterized by elevated concentrations of As (0.73–3.96 wt% As_2O_5), which correlate positively with the REE content (Fig. 6b). Yttrium is the most abundant REE, ranging from 0.33 to 2.47 wt% Y_2O_3. The green powellite crusts occurring on quartz crystals in open fractures contain >99 mol% $CaMoO_4$ and <0.05 wt% As_2O_5 (Fig. 6a).

The excellent inverse correlation between MoO_3 and WO_3 ($R^2 = 0.99$ for 75 analyses) is consistent with the single-site substitution

$$WMo_{-1}. \quad (1)$$

The data further show an excellent positive correlation between ΣREE and As (Fig. 6b). Because REE are accommodated on the Ca site (Cottrant 1981), and As most probably substitutes for Mo (or W), the correlated variation of As and REE must be the result of a coupled substitution. The latter is best described by the exchange vector

$$REE^{3+}\ As^{5+}\ Ca^{2+}_{-1}\ (Mo,W)^{6+}_{-1}. \quad (2)$$

The slope of the linear regression between ΣREE and As, however, is only +0.72 (Fig. 6b), a feature that could be explained by the fact that not all REE were analyzed (particularly Ce). Substitution 2 requires As to be present as As^{5+}; this oxidation state is to be expected when the mineral occurs within oxidized ores (hematite, arsenates).

During the detailed study of crystal Se2/10 (cf. Fig. 5, Table 3), two different compositional trends were found for stages A and B_1 (B_2 could not be analyzed because the zone is too narrow for EMP analysis). Analyses of stage-A scheelite-powellite plot along a line relating the As, Mo, and W contents (Fig. 5c). The As content is

TABLE 3. Selected EMP analyses of sample Se10/2

Analysis no.	1	2	3	4	5	6	1σ [%]*
Zone (Pt. N°)	B1 (no. 141)	B1 (no.140)	B1 (no. 146)	B1 (no. 147)	A1	A2 (Minimum–Maximum)	
Average of	1	1	1	1	6	8	
CaO	21.57	20.80	19.94	21.24	24.42	22.65 (22.32–23.05)	0.8
WO_3	56.33	54.34	52.15	53.44	30.80	41.06 (38.92–43.62)	1.9
MoO_3	18.65	18.59	16.60	18.51	43.17	31.83 (30.02–32.66)	1.4
As_2O_5	1.19	2.49	3.96	2.39	0.82	1.89 (1.57-2.16)	1.8
Y_2O_3	0.52	1.13	2.47	1.03	0.34	0.92 (0.67–1.11)	1.8
Nd_2O_3	0.536	0.439	0.712	0.493	0.175	0.440 (0.391–0.493)	1.4
La_2O_3	0.470	0.466	0.362	0.536	0.175	0.291 (0.243–0.335)	1.8
Sm_2O_3	0.098	0.066	0.120	0.029	0.022	0.074 (0.053–0.089)	1.2
Dy_2O_3	0.092	0.070	0.120	0.086	0.018	0.086 (0.067–0.107)	1.0
Er_2O_3	0.053	0.053	0.064	0.065	0.012	0.045 (0.036–0.055)	1.0
Sum	*99.51*	*98.44*	*96.50*	*97.82*	*99.95*	*99.29*	
Formula proportions based on 4 O atoms							
Ca	0.995	0.963	0.943	0.997	0.990	0.973	
Y	0.012	0.026	0.058	0.024	0.007	0.020	
Nd	0.008	0.007	0.011	0.008	0.002	0.006	
La	0.007	0.007	0.006	0.009	0.002	0.004	
Sm	0.001	0.001	0.002	0.0004	0.0003	0.001	
Dy	0.001	0.001	0.002	0.001	0.0002	0.001	
Er	0.001	0.001	0.001	0.001	0.0001	0.001	
Sum	*1.025*	*1.006*	*1.023*	*1.040*	*1.002*	*1.006*	
ΣREE	*0.030*	*0.043*	*0.080*	*0.043*	0.012	0.033	
W	0.629	0.609	0.597	0.607	0.302	0.427	
Mo	0.335	0.335	0.306	0.338	0.682	0.533	
As	0.027	0.056	0.092	0.055	0.016	0.040	
Sum	*0.991*	*1.000*	*0.995*	*1.000*	*1.000*	*1.000*	
W/(W+Mo)	0.65	0.65	0.66	0.64	0.31	0.44	

Notes: For location of analyses, see Figure 4a.
* Typical 1σ error resulting from the counting statistics for a single analysis.

correlated positively with W/Mo and, therefore, substitutions 1 and 2 must take place simultaneously. B_1 compositions lie along a line of constant W/Mo, but vary with respect to As. EMP analyses of three other crystals displaying two growth stages yielded similar results. On element distribution maps, the As content appears quite homogeneous in zone B (Fig. 5d), and the W content (Fig. 5e) mimics the BSE image. Figure 5d reveals that the As content of the B_1 and B_2 zones is similar to that of the A_2 zone (see also Fig. 5c). The apparent homogeneity of the As concentration observed on the element distribution map of zone B is in apparent contradiction with the quantitative EMP analyses; this contradiction will be addressed below.

REE CHARACTERISTICS OF SCHEELITE-POWELLITE

Analytical methods

Information on the REE characteristics of scheelite-powellite was obtained by EMP and isotope dilution (ID) analysis, and by luminescence spectroscopy. With a tightly focused electron beam, the volume of electron-matter interaction is approximately 0.5 and 6 μm^3 at 15 and 25 kV, respectively (program Monte Carlo by John Pilling, Michigan Technological University, Houghton). Therefore, by using the EMP, it is possible to obtain in-situ analyses of the different zones (except for the narrow B_0 and B_2 veinlets). However, due to the relatively low REE concentrations in the samples and because of X-ray interferences, only a limited set of REE could be determined. A larger set of REE can be determined by ID analysis, but the small size of the zonations precluded analysis of the different generations of scheelite-powellite. ID data, therefore, correspond to bulk analyses carried out in the present case on 0.25 mm^3 of powdered material. Similarly, luminescence spectroscopy yields bulk analyses, but this method, unlike EMP and ID analysis, detects only those REE^{3+} cations that occur on specific crystallographic sites in a given mineral (e.g., on the Ca site in scheelite-powellite; Cottrant 1981). Quantitative evaluation of the luminescence spectra is afflicted by many difficulties, particularly in Mo-rich scheelites (Uspensky et al., 1998). However, comparison of the unknown spectra with those of synthetic scheelite standards allowed us to identify individual REE peaks and thereby to discuss the REE patterns qualitatively. In our study, we have used thermal X-ray luminescence (XLT) spectroscopy, a method that yields better peak/background ratios than the standard X-ray activated luminescence spectroscopy (Uspensky et al. 1998). The spectra were collected at 250 °C using X-ray excitation at 30 kV, 60 μA (for details of analytical procedure, see Uspensky et al. 1998). Three different samples (including one used for subsequent ID analysis) of single scheelite-powellite grains (0.1–0.3 mm across) were analyzed.

Results

The chondrite-normalized REE pattern obtained from the EMP data (Fig. 7a) is similar to that constructed from the ID data (Fig. 7b, Table 4), and is characterized by an enrichment in light REE (LREE) and variable La/Nd ra-

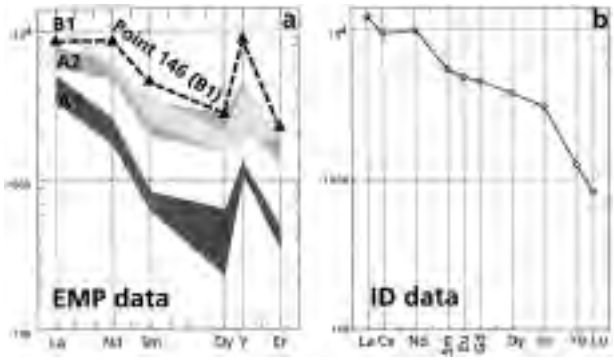

FIGURE 7. (**a**) Chondrite-normalized REE pattern for sample Se2/10; data from EMP analyses (Table 3); (**b**) Chondrite-normalized REE pattern for scheelite-powellite grain JB311; data from ID analysis (Table 4). Chondrite data are from Taylor and McLennan (1985).

tios. The REE content of zone B_1 is comparable to that of zone A_2, with the exception of La, which is much higher in B_1. One analysis within B_1 (point no. 146) is distinct, because it displays high values for all the REE, especially for Y (Fig. 7a). All three XLT spectra generated for scheelite-powellite are very similar. One example is shown in Figure 8, which displays peaks related to REE^{3+} at the position typical for scheelite. This indicates that the REE are present, at least in part, on a structural site (Ca site) of the scheelite-powellite lattice, and not in submicroscopic inclusions. The XLT spectra are characterized by an enrichment in LREE (as represented by the Sm^{3+} line), in agreement with the ID data. The intensity distribution of the Er^{3+}, Tb^{3+}, and Dy^{3+} peaks is typical for scheelite from stratabound metamorphic deposits (see Uspensky et al. 1998) although the high Mo content and the extremely strong LREE enrichment are unique (Uspensky, unpublished database of 2000 spectra from 300 localities).

SCHEELITE-POWELLITE AT THE SCALE OF THE TRANSMISSION ELECTRON MICROSCOPE

Although XLT spectroscopy revealed that the REE are at least partly incorporated into a structural site of scheelite-powellite, the possible presence of submicroscopic REE-rich inclusions, particularly of paraniite-(Y), could not be precluded. Three different hypotheses had to be tested: (1) the entire amount of As and REE is distributed randomly on the (Mo,W) and Ca sites of scheelite-powellite, respectively; (2) layers of $YAsO_4$ are distributed randomly in the scheelite-powellite matrix; and (3) small crystals of paraniite-(Y) occur in the scheelite-powellite matrix. Transmission electron microscopy (TEM) has been used to evaluate the two latter possibilities.

Analytical methods

TEM samples were prepared from polished thin sections that had been studied previously by BSE imaging. The ion-beam thinned and carbon-coated disks were mounted on a double tilt stage for use in a Philips CM 20 microscope operated at 200 keV. The high-resolution TEM (HRTEM) images were recorded near Scherzer defocus values at original magnifications of 390 000×. Contrast simulations were obtained with the EMS program package of Stadelmann (1987). Quantitative chemical analyses were carried out by Analytical Electron Microscopy (AEM). Data were collected using an EDAX 9800 Plus energy-dispersive X-ray (EDX) system attached to the TEM column. The EDX data were quantified using the thin film approximation of Cliff and Lorimer (1975), which assumes that absorption and fluorescence of the X-rays while traversing the thinned edge of the sample are negligible.

The original paraniite-(Y) crystal used by Demartin et al. (1992) for the structure analysis is about 100 μm in length and was split into two pieces. One piece was kept as part of the type material, the second was crushed, dispersed on holey carbon grids, and used in conjunction with a natural powellite sample as a standard to determine the Cliff-Lorimer *k*-factors. Ca was used as a reference element. Both standard and samples were analyzed using a 30–50 nm beam and life times of 100–200 s. The Ca peak averaged between 6000 and 10 000 counts. Average counting statistical errors are 0.8% for W and Ca, 1.0% for As, and 1.5% for Mo and Y. Factors such as absorption, homogeneity of the standards, and topography of the

TABLE 4. Isotope dilution data for scheelite-powellite from Fianel

Element	[ppm]	2σ (%)
La	2990	2
Ce	5904	1
Nd	4653	1
Sm	834.3	1
Eu	279.1	1
Gd	926.6	2
Dy	952	1
Er	507.8	1
Yb	207.1	1
Lu	20.58	2

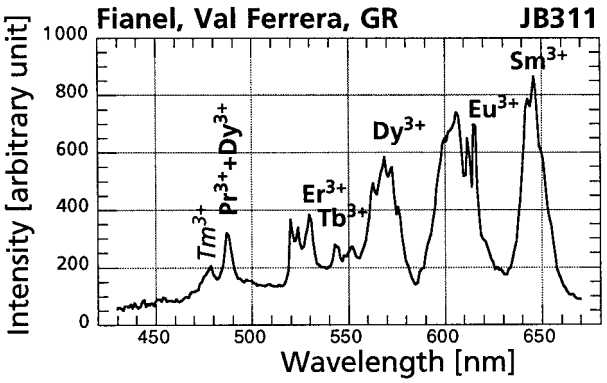

FIGURE 8. Thermal X-ray luminescence spectrum of scheelite-powellite grain JB311. Analytical conditions: 250 °C, 30 kV, and 60 μA.

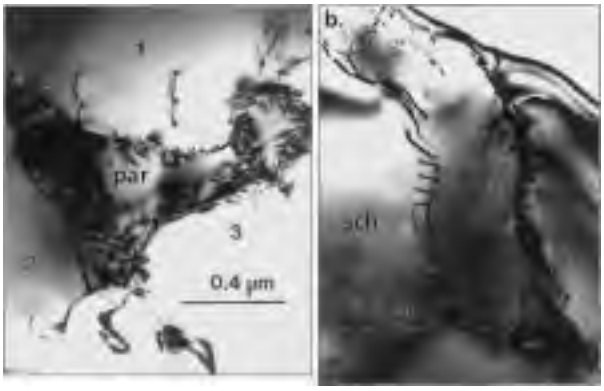

FIGURE 9. (**a**) TEM brightfield image of a paraniite-(Y) (par) grain at a triple junction of three scheelite subgrains (numbered). Arrow points to accumulated dislocations delimiting the subgrains. (**b**) TEM brightfield image of a paraniite-(Y) grain. The defects between scheelite-powellite (sch) and paraniite-(Y) indicate that the latter acted as an anchor during deformation.

sample surface will all degrade the analytical precision and accuracy, but are difficult to assess quantitatively. The precision for the major elements is thought to be no better than 5% of the amount measured (Livi and Veblen 1987).

Results

The TEM investigations revealed high dislocation densities ($>10^8$–10^9/cm^2) for scheelite-powellite of stages A and B. The dislocations commonly form subgrain boundaries. Along such subgrain boundaries of the late W-rich generation (stage B), and particularly in triple junctions, small grains of paraniite-(Y) have been identified (Fig. 9). The amount of paraniite-(Y) present in the stage-B scheelite-powellite matrix is probably below 1 vol%. All the paraniite-(Y) crystals (0.1–1 μm across) examined by selected area electron diffraction (SAED) and HRTEM show a topotactic relationship with the matrix scheelite-powellite whereby $c_{Par}//c_{Sch}$ and $a_{Par}//a_{Sch}$ (Fig. 10a). The boundaries between scheelite-powellite and paraniite-(Y) are irregular and characterized by misfit dislocations (Fig. 10a). No polysomatic faults in the scheelite-$YAsO_4$ layer stacking of paraniite-(Y) were detected in HRTEM images and no random $YAsO_4$ layers were found in the scheelite-powellite matrix (Fig. 10b). The same situation was observed for the type material of paraniite-(Y), in agreement with the crystal structure determination of Demartin et al. (1994).

As revealed by the AEM data (Table 5), the main difference between the composition of paraniite-(Y) from Fianel and that of the type specimen is the partial replacement of W by Mo in the Fianel sample (Fig. 11a). The W/(W+Mo) ratio in paraniite-(Y) is slightly higher than in the stage-B matrix scheelite-powellite (0.73 and 0.65, respectively, Table 5, see also Fig. 11b). In the type specimen, Y and As are substituting into the scheelite layer, whereas in the Fianel paraniite-(Y) a small amount of Ca and (W,Mo) are incorporated into the $YAsO_4$ layer (Figs. 11a and 11b, Table 5). The sum of the Ca site cations does not take into account all REE but only Y, and is therefore a little low. Peaks corresponding to Ce and Nd appear on the AEM spectra of paraniite-(Y), but are absent in the spectra of matrix scheelite-powellite. A reliable quantification of Ce and Nd is difficult due to their low concentrations, and hence was not performed.

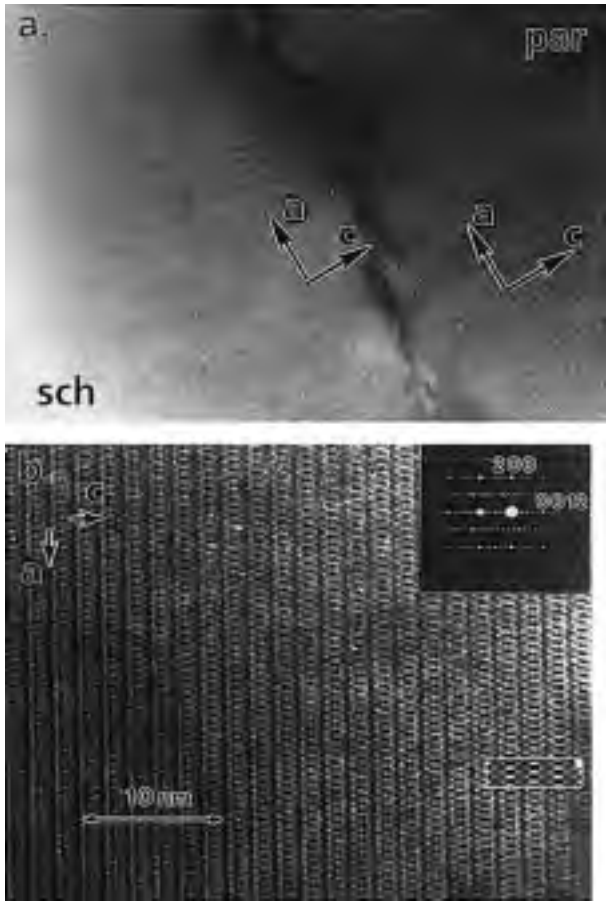

FIGURE 10. (**a**) [010] HRTEM image of a boundary between scheelite and paraniite-(Y). (**b**) [010] HRTEM image of paraniite-(Y) with the corresponding SAED pattern in the upper right corner. The inset in the lower right part of the image is a contrast simulation for a crystal thickness of 7.5 nm and a defocus of −15 nm.

DISCUSSION

Origin of the mineral association

In Val Ferrera, scheelite-powellite thus far has been only identified in the breccia lens at Fianel. Geochemical studies show, however, that all Fe and Fe-Mn ores within the marbles of Val Ferrera display significant positive anomalies in Mo, W, As, Sb, and Be concentrations (enriched 10 to >100× relative to the unmineralized rocks; Brugger 1996). At Fianel, synkinematic As, Be, and Sb minerals occur in the main schistosity (S_1) and thus, these elements must have

TABLE 5. AEM analyses of two paraniite-(Y) crystals and coexisting scheelite-powellite from Fianel in comparison to the analysis of the type material of paraniite-(Y)

Average no. of analyses	Type*	Paraniite 1		Paraniite 2		Scheelite†	
		4	1σ	8	1σ	6	1σ
CaO	12.35	15.5	(0.6)	15.4	(0.7)	21.4	(0.5)
WO_3	51.61	48.2	(0.7)	45.0	(0.6)	55.3	(0.3)
MoO_3	<0.10	13.0	(0.6)	10.6	(0.7)	18.4	(0.2)
Y_2O_3	16.15	10.1	(0.5)	12.5	(0.9)	1.0	(0.4)
As_2O_5	16.92	11.7	(0.6)	15.1	(0.7)	2.3	(0.4)
Formula proportions based on 4 O atoms (paranaiite) and 12 O atoms (scheelite)							
Ca	1.64	2.13		2.10		0.99	
W	1.82	1.60		1.48		0.62	
Mo		0.70		0.56		0.33	
Y	1.36	0.69		0.85		0.02	
As	1.18	0.78		1.00		0.05	
Ca+Y	3.00	2.82		2.95		1.01	
W+Mo+As	3.00	3.08		3.04		1.00	
W/(W+Mo)	1.00	0.70		0.73		0.65	

* EMP analysis of paraniite-(Y) type material (Demartin et al. 1994), which additionally contains 0.70 wt% Gd_2O_3, 1.87 wt% Dy_2O_3, 1.37 wt% Er_2O_3, 0.81 wt% Yb_2O_3, and 0.25 wt% UO_2.

† Scheelite (stage B) in contact with paraniite 2.

been introduced no later than during the main Tertiary metamorphic event (D_1). Structural observations show that brecciation predates the main deformation (D_1) in the pink dolomite breccia. This breccia, therefore, may represent a syngenetic ''hydrothermal eruption breccia'' in the sense of Hedenquist and Henley (1985); alternatively, it may be linked to the dissolution of minerals such as anhydrite during diagenesis, as observed in modern sea-floor exhalative deposits (Humphris et al. 1995**)**.

The quartz+dolomite veins that contain the Be, Mo, W, Sb, As, F, and P minerals were formed in the pink dolomite breccia after D_1 and, thus, are also a product of the Tertiary metamorphism. Textural evidence indicates a co-precipitation of quartz, dolomite, scheelite-powellite, and beryl during the opening of the veins. These veins do not propagate into the surrounding hematite-quartz-carbonate ores, because the competent breccia lenses exhibited brittle behavior in contrast to the embedding ores. The distinct mineral association hosted by the veins in the breccia may therefore be related to a special, pre-metamorphic geochemical character of the breccia, and to the rheologic properties of the breccia, which allowed the opening of many fractures where minerals could crystallize. The occurrence of fluorapatite and carbonate in the veins provides evidence for the presence of PO_4^{3-}, F^-, and CO_3^{2-} in the fluid. The availability of strong ligands such as F greatly enhances the hydrothermal mobility of REE (e.g., Haas et al. 1995). The oxidized nature of the Fe-Mn mineralization prevented the removal of Mo as molybdenite, and thus was responsible for the appearance of scheelite-powellite.

The element association in the veins (Be, Mo, W, Sb, As, F, P) and the inferred chemical composition of the mineralizing fluid (elevated PO_4^{3-}, F^-, and CO_3^{2-} contents and high Eh) mimic the geochemistry of the embedding hematite-quartz-carbonate ores. The LREE enrichment displayed by scheelite-powellite reflects a general characteristic of the Fianel ores (Brugger 1996). Therefore, it appears that all the elements constituting the vein minerals have a local origin (i.e., from the breccia with a more or less important component from the surrounding ore). The veins, thus, represent an example of local remobilization during the Alpine deformation.

Paraniite-(Y) and the metasomatic replacement of scheelite-powellite

In stage-A scheelite-powellite, As and REE are in solid solution within the scheelite-powellite structure. In stage-B scheelite-powellite, however, a portion of the As and REE measured by the EMP is hosted by sub-microscopic paraniite-(Y) inclusions that probably comprise <1 vol% of the matrix. The volume of the largest paraniite-(Y) crystals is about 0.1 μm^3 (Fig. 9a:1 × 0.3 × 0.3 μm). If the entire grain would lie within the EMP analysis volume of 0.5 μm^3 at 15 kV, it would account for 20% of this volume. Because paraniite-(Y) and the surrounding scheelite-powellite matrix contain approximately 14 and 2 wt% As_2O_5, respectively (Table 5), and because both minerals have similar densities, the resulting EMP analysis would show approximately 4.5 wt% As_2O_5, a value that is in good agreement with the maximum measured value of 3.96 wt% As_2O_5. The latter was found in analysis no. 146 (Table 3), which further exhibits a significant enrichment in Y relative to other scheelite-powellite analyses of stage B_1 (cf. Fig. 7a). This Y enrichment must result from the presence in the analysis volume of paraniite-(Y), which strongly concentrates Y.

We should bear in mind that the chances of including an entire paraniite-(Y) grain during an analysis are low. If, as noted previously, paraniite-(Y) occupies a volume of ~1% of the scheelite-powellite matrix, a single cube of scheelite-powellite 15 μm on a side would contain 270 cubes of paraniite-(Y) 0.5 μm on a side. In this case, the probability of including one corner of a paraniite-(Y) cube within a semi-spherical analysis volume with a radius of 0.6 μm is only 8–9%. The probability drops to 1–2% for the inclusion of three corners, a situation where no more than half of the paraniite-(Y) crystal is contained within the analysis volume. Thus, in the As distribution map shown in Figure 5d, only a few isolated pixels will show elevated As contents as a result of the presence of paraniite-(Y). This explains why the B-zone scheelite-powellite appears homogeneous on the X-ray map at the scale used (Fig. 5d), although EMP spot analyses show significant variation in As content (cf. Fig. 5c).

The fluid responsible for the metasomatic replacement of stage-A by stage-B scheelite-powellite probably displayed the following characteristics: (1) higher W activity relative to Mo than during stage A; (2) As activity corresponding to the highest value found in stage A; and (3) REE contents marked by a high La (and probably Ce) content relative to the stage-A fluid (Fig. 7). The high

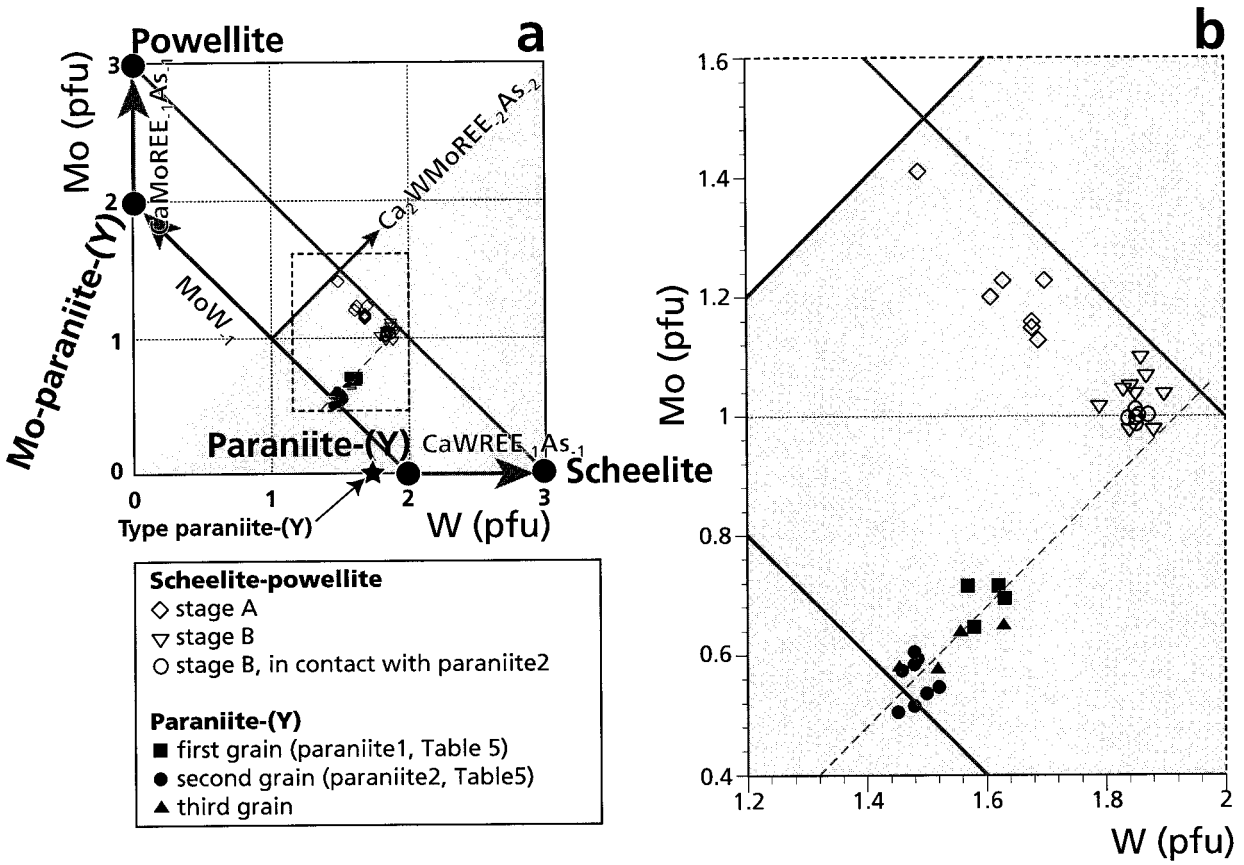

FIGURE 11. AEM analyses of scheelite-powellite and paraniite-(Y). The pfu values for scheelite-powellite were multiplied by three. (**a**) Complete diagram, showing the W and Mo end-members of the two minerals as well as the main substitutions; (**b**) enlargement of the area containing the Fianel data (marked in Fig. 11a). Scheelite-powellite at the vicinity of paraniite-(Y) grains has low Mo contents, and was attributed to stage B.

dislocation density found in both generations of scheelite-powellite indicates that the metasomatic replacement of stage-A scheelite-powellite by a W-rich fluid happened before the end of the deformation events. The paraniite-(Y) grains acted as anchors for subgrain boundaries during the deformation, and therefore also must have been formed prior the last deformation (i.e., most likely before the end of D_3). Although we do not have more precise indications about the relative ages of the metasomatic replacement and the crystallization of paraniite-(Y), the conclusion that both events are related and occurred at the same time seems justified.

During the metasomatic replacement, scheelite-powellite was still able to incorporate high amounts of REE and As into its structure. The formation of the paraniite-(Y) (par) crystals during stage B by destabilization of Y- and As-rich scheelite-powellite (sch) of stage A can be written schematically as

$$\text{sch-A} + \text{fluid1} = \text{sch-B} + \text{par-B} + \text{fluid2} \qquad (3)$$

if we assume the presence of a fluid. Fig. 7a suggests that formation of stage-B_1 scheelite-powellite has occurred without major input of HREE from the fluid. If we suppose that no Y was added by the fluid, the mass balance for Y is given by:

$$Y_{A_{sch}} = (1 - v)Y_{B_{sch}} + vY_{B_{par}} \qquad (4)$$

because $\rho_{sch} \approx \rho_{par}$. With $Y_{B_{sch}}$ = 1.0 wt% Y_2O_3 (Table 5), $Y_{B_{par}}$ = 11.3 wt% Y_2O_3 (mean of the two analyses in Table 5), the relative volume (v) of paraniite-(Y) is 0.3% and 1.0% for $Y_{A_{sch}}$ = 1.03 and 1.10, respectively (1.03 and 1.10 wt% Y_2O_3 are within the $Y_{A_{sch}}$ range for A_2, see Table 3). These values for v are consistent with the volume percentage inferred from the TEM investigations.

Stage-B scheelite is enriched in LREE, however. The presence of Nd and Ce peaks on the AEM spectra of paraniite-(Y) show that this mineral does not only incorporate HREE, but also small amounts of LREE. Most of the LREE, however, have to be incorporated in scheelite-powellite, and stage-B scheelite-powellite could indeed host more LREE than stage-A scheelite-powellite (Fig. 7a). If scheelite-powellite of stage A is nearly saturated with respect to the total REE content, then the equilibration of this scheelite-powellite with a LREE-rich fluid could induce the release of HREE, which are subsequently incorporated in paraniite-(Y). The same reasoning may

be applied to As, but there is no evidence that stage B_1 is richer in As than stage A_2 (Fig. 5c).

The existence of LREE- and As-rich fluids in the Fe-Mn ores of Val Ferrera is not only indicated by the occurrence of paraniite-(Y). Within the pink dolomite breccia, such a fluid is also documented by As-rich rims in fluorapatite, and by recrystallized areas in fluor-roméite (Brugger et al. 1997). A similar situation was observed at the nearby Starlera deposit (located 3 km away), which contains a retrograde mineral association with cerian-antimonian-roméite, bergslagite, and arsenian fluorapatite. It appears that a LREE- and As-rich fluid has some regional significance. Therefore, we can conclude that, at some stage during the retrograde metamorphism in Val Ferrera (pre- to syn-D_3), conditions favorable for the mobilization of As and LREE were achieved. In the Binntal region (Western Central Alps), similar retrograde metamorphic As- and REE-rich fluids were inferred to be responsible for the formation of numerous uncommon REE-bearing arsenates, arsenites, and As-bearing silicates (Graeser and Roggiani 1976; Demartin et al. 1994; Krzemnicki 1996; Knill 1996).

Acknowledgments

We thank S. Graeser and G. Schreurs for constructive discussions; L. Raimbault and B. Guy for their thorough reviews; T. Mummenthaler for collecting; and N. Meisser for identifying bergslagite; B. Hofman for the determination of chernovite-(Y); C.M. Gramaccioli for kindly providing the type material of paraniite-(Y); R. Oberhänsli for giving us a powellite standard; and D.Z. Zuralev for the ID analysis. We also express our gratitude to L. Diamond (EMP Laboratory, Bern, supported by Schweizerischer Nationalfonds grant no. 21-26579.89), R. Guggenheim (SEM Laboratory, Basel), J. Chevallier (TEM facility, Aarhus), and C. Hadidiacos (EMP Laboratory, Washington, D.C.) for giving us access to their laboratories. The help of all these colleagues has been invaluable. This work was supported by the Schweizerischer Nationalfonds (grant no. 2000-43350.95).

References cited

Brugger, J. (1996) The Fe, Mn, (V, Sb, As, Be, W) deposits of Val Ferrera (Graubünden, Switzerland). Ph.D. dissertation, University of Basel, Switzerland.

Brugger, J., Gieré, R., Graeser, S., and Meisser, N. (1997) The crystal chemistry of roméite. Contributions to Mineralogy and Petrology, 127, 136–146.

Cliff, G. and Lorimer, G.W. (1975) The quantitative analysis of thin specimens. Journal of Microscopy, 103, 203–207.

Cottrant, J.F. (1981) Cristallochimie et géochimie des terres rares dans la scheelite: Application à quelques gisements français. Ph.D. dissertation, University of Paris-VI, France.

Dana, D. and Dana, E.S. (1951) The system of Mineralogy. 7th edition, rewritten and enlarged by Charles Palache, Harry Berman and Clifford Frondel. Wiley, New York.

Demartin, F., Gramaccioli, C.M., and Pilati, T. (1992) Structure of a new natural tungstate arsenate, $[Ca_2Y(AsO_4)(WO_4)_2]$, structurally related to scheelite. Acta Crystallographica, C48, 1357–1359.

———(1994) Paraniite-(Y), a new tungstate arsenate mineral from Alpine fissures. Schweizerische Mineralogische und Petrographische Mitteilungen, 74, 155–160.

Goldin, B.A., Yushkin, N.P., and Fishman, M.V. (1968) New mineral names: A new yttrium mineral, chernovite. American Mineralogist, 53, 1777.

Graeser, S. (1974) Mineral-Neufunde aus der Schweiz und angrenzenden Gebieten. Schweizer Strahler, 3(7), 265–277.

Graeser, S. and Roggiani, A.G. (1976) Occurrence and genesis of rare arsenate and phosphate minerals around Pizzo Cervandone, Italy/Switzerland. Rendicontri della Societa Italiana di Mineralogia e Petrologia, 32, 279–288.

Haas, J.R., Shock, E.L., and Sassani, D.C. (1995) Rare earth elements in hydrothermal systems: estimates of standard partial molal thermodynamic properties of aqueous complexes of the rare earth elements at high pressures and temperatures. Geochimica et Cosmochimica Acta, 59, 21, 4329–4350.

Hänni, H.A. (1980) Mineralogische und Mineralchemische Untersuchungen an Beryll aus alpinen Zerrklüften. Ph.D. dissertation, University of Basel, Switzerland.

Hedenquist, J.W. and Henley, R.W. (1985) Hydrothermal eruptions in the Waiotapu geothermal system, New Zealand: their origin, associated Breccias, and relation to precious metal mineralization. Economic Geology, 80, 1640–1668.

Hsu, L.C. and Galli, P.E. (1973) Origin of the scheelite-Powellite serie of minerals. Economic Geology, 68, 681–696.

Humphris, S.E., Herzig, P.M., Miller, D.J., Alt, J.C., Becker, K., Brown, D., Brügmann, G., Chiba, H., Fouquet, Y., Gemmel, J.B., Guerin, G., Hannington, M.D., Holm, N.G., Honnorez, J.J., Iturrino, G.J., Knott, R., Ludwig, R., Nakamura, K., Petersen, S., Reysenbach, A.-L., Rona, P.A., Smith, S., Sturz, A.A., Tivey, M.K., and Zhao, X. (1995) The internal structure of an active sea-floor massive sulphide deposit. Nature, 377, 713–715.

Ivanova, G.F., Bannykh, L.N., Ignatenko, K.I., and Kluger, F. (1987) Trace components in scheelite from deposits of various genetic types. Geochemistry International, 24, 12, 1–20.

Knill, M.D. (1996) The Pb-Zn-As-Tl-Ba-deposit at Lendenbach, Binn Valley, Switzerland. Beiträge zur Geologie der Schweiz, Geotechnische Serie, 90. Lieferung, 74 p.

Krzemnicki, M. (1996) Mineralogisch-krystallchemische Untersuchungen im Bereich der Monte Leone Decke. Ph.D. dissertation, University of Basel, Switzerland.

Livi, K.J.T. and Veblen, D.R. (1987) ''Eastonite'' from Easton, Pennsylvania: A mixture of phlogopite and a new form of serpentine. American Mineralogist, 72, 113–125.

Raimbault, L., Baumer, A., Dubru, M., Benkerrou, C., Croze, V., and Zahm, A. (1993) REE fractionation between scheelite and apatite in hydrothermal conditions. American Mineralogist, 78, 1275–1285.

Richard, A., Dabrowski, H., and Michel, R. (1981) Contribution à l'étude des éléments en traces de quelques scheelites des Alpes. Géologie Alpine, 57, 109–114.

Schmid, S.M., Pfiffner, O.A., and Schreurs, G. (1997) Rifting and collision in the Penninic zone of eastern Switzerland. In A. Pfiffner, Ed., Deep structure of the Swiss Alps-Results from NFP/PNR 20. Birkhäuser AG, Basel, 160–185.

Semenov, Y.I. (1963) Rare earths mineralogy (in Russian). Izd. AN SSSR, Moscow, 412 p.

Stadelmann, P.A. (1987) EMS-A software package for electron diffraction analysis and HREM image simulation in material sciences. Ultramicroscopy, 21, 131–146.

Stucky, K. (1960) Die Eisen-und Manganerze in der Trias des Val Ferrera. Beiträge zur Geologie der Schweiz, Geotechnische Serie, 37. Lieferung, 67 p.

Taylor, S.R. and McLennan, F.S. (1985) The continental crust: its composition and evolution. Blackwell Science Publications, Oxford, 312 p.

Trümpy, R. (1980) Geology of Switzerland, a guide book. Part A: An outline of the geology of Switzerland. Schweizerische geologische Kommission, Wepf, Basel, 104 p.

Tyson, R.M., Hemphill, W.R., and Theisen, A.F. (1988) Effect of W:Mo ratio on the shift of exitation and emission spectra in the scheelite-powellite series. American Mineralogist, 73, 1145–1154.

Uspensky, E., Brugger, J., and Graeser, S. (1998) REE geochemistry systematics of scheelite from the Alps using luminescence spectroscopy: from global regularities to facies control. Schweizerische Mineralogische und Petrographische Mitteilungen, 78/1, 38–54.

Zalkin, A. and Templeton, D.H. (1964) X-ray diffraction refinement of the calcium tungstate structure. Journal of chemical physics, 40(2), 501–506.

Manuscript received July 7, 1997
Manuscript accepted April 10, 1998
Paper handled by Gray E. Bebout